Chemically Functionalized Carbon Nanotubes with Pyridine Groups as Easily Tunable N-Decorated Nanomaterials for the Oxygen Reduction Reaction in Alkaline Medium

Giulia Tuci,[†] Claudio Zafferoni,[‡] Andrea Rossin,[†] Antonella Milella,[§] Lapo Luconi,[†] Massimo Innocenti,[‡] Lai Truong Phuoc,[∥] Cuong Duong-Viet,[∥] Cuong Pham-Huu,[∥] and Giuliano Giambastiani*[,†,⊥]

[†]Institute of Chemistry of OrganoMetallic Compounds, ICCOM-CNR and INSTM Consortium, 50019 Sesto F.no, Florence, Italy

[‡]Department of Chemistry, University of Florence, 50019 Sesto F.no, Florence, Italy

[§]Department of Chemistry, University of Bari, 70126 Bari, Italy

[∥]Institut de Chimie et procédés pour l'Energie, l'Environnement et la Santé (ICPEES), UMR 7515 CNRS-Université de Strasbourg, Strasbourg, France

[⊥]Kazan Federal University, 420008 Kazan, Russian Federation

🅂 Supporting Information

ABSTRACT: We report on the N-decoration of multiwalled carbon nanotubes (MWCNTs) via chemical functionalization under mild reaction conditions. The introduction of tailored pyridinic functionalities as N-containing edge-type group mimics generates effective catalysts for the oxygen reduction reaction (ORR) in an alkaline environment. The adopted methodology lists a number of remarkable technical advantages, among which is an easy tuning of the electronic properties of N-containing groups. The latter aspect further increases the level of complexity for the rationalization of the role of the N-functionalities on the ultimate electrochemical performance of the as-prepared metal-free catalysts. Electrochemical outcomes crossed with the computed electronic charge density distributions on each scrutinized pyridine group have evidenced the central role played by the N-chemical environment on the final catalyst performance. Notably, small variations of the atomic charges on the N-proximal carbon atoms of the chemically grafted heterocycles change the overpotential values at which the oxygen reduction reaction starts. The protocol described hereafter offers an excellent basis for the development of more active metal-free electrocatalysts for the ORR. Finally, the as-prepared catalytically active materials represent a unique model for the in-depth understanding of the underlying ORR mechanism.
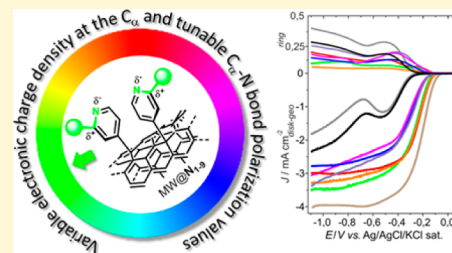
INTRODUCTION

Efficient and low-cost electrocatalysts capable of facilitating the sluggish cathodic oxygen reduction reaction (ORR) are at the heart of renewable energy technologies based on fuel cells and other electrochemical energy devices. The prohibitive cost of the platinum-group metal (PGM)-based electrocatalysts, together with their limited reserves in nature, constitute the major drawback to their sustainable commercial application in several technological fields. Despite their outstanding electrocatalytic performance in the ORR, Pt-based electrocatalysts can suffer from severe poisoning effects (such as gas adsorption or fuels crossover) which affect their durability and limit their practical application sphere.[1−4] Along with recent intensive research efforts in reducing or replacing Pt-based electrocatalysts in ORR,[5] light-heteroelement doped carbon nanomaterials (CNMs) with at least one dimension tailored at the nanometer scale have raised the interest of the catalysis and material science community.[6−10] In particular, nitrogen-doped CNMs (N-CNMs) have been intensively investigated, in light of their remarkable electrochemical properties for the ORR in

an alkaline environment.[8,11,12] Moreover, the presence of an adequate number of catalytically active sites exposed on materials typically featured by high surface area and excellent electrical conductivity makes them attractive single-phase catalysts with no need of any additional conductive support. Although the ORR in alkaline media is catalyzed by a wide variety of pure carbon-based electrocatalysts such as glassy carbon (GC),[13,14] active carbon,[15] carbon nanotubes,[16] graphene, and other related carbon-based materials,[6,17] the absence of alien atoms in the sp^2 C-network translates into a simple $2e^-$ reduction process featured by moderate current densities (J) and low onset potentials, with the generation of HO_2^- ions as the main oxidation product. On the contrary, an appropriate CNM engineering through a light-heteroelement doping (mostly N-doping) has led to the obtainment of more performing metal-free electrocatalysts fostering a prevalent $4e^-$

reduction process with OH^- ions as the major oxidation product. Intensive studies in the field have contributed to the discovery of excellent N-CNM-based, metal-free systems active in the ORR, showing similar and even better electrocatalytic activity, long-term stability, and tolerance to crossover effects than that of expensive platinum-based electrocatalysts.[18−25] Since the first seminal report by Dai and co-workers in 2009,[18] a huge effort has been made to prepare either monodimensional (1D) or bidimensional (2D) N-CNMs and to fully exploit their catalytic ability on both a theoretical[26−30] and experimental[6−10] ground. Among the synthetic methods used for their preparation, chemical vapor deposition (CVD) still remains the most effective and widely used technique,[31,32] although other approaches such as CNMs annealing in the presence of different nitrogen sources,[33,34,53] chemical reduction/doping with selected N-containing reducing agents,[7,35,36] or direct carbonization of N-containing organic precursors[37,38,60] constitute valuable and alternative synthetic paths. However, none of the above-mentioned approaches fulfill the requirement of a protocol for an effective tailoring of the introduced N-functionalities.

Although the role of nitrogen doping and the nature of the "catalytically active" nitrogen sites in these complex carbon nanostructures still represent an intensive matter of debate,[6−10] it seems clear that the inclusion of nitrogen(s) in the honeycomb carbon structure, besides inducing remarkable modifications of the physicochemical properties of the undoped 1D and 2D materials (such as structure, electrical conductivity, surface properties, and oxidation stability), breaks the electroneutrality of the Csp^2 network, thus generating carbon active sites proximal to the heteroatom[39] which take part in the molecular oxygen activation and subsequent $O\!=\!O$ bond breaking.[40] Indeed, a net redistribution of the charge density around the nitrogen atoms improves the material oxygen adsorption properties and facilitates the occurrence of the electrochemical oxygen reduction;[41,53] an appropriate balance between a moderate oxygen binding energy and a highly localized electron density around the active site seems to be crucial for getting highly performing ORR catalysts.[18,42] Independent research groups have recently discussed how the introduction of N atoms into the network of a carbon-based nanomaterial would increase the electronic density of states near the Fermi level, thus facilitating the electron transfer from the electronic bands of the C network to the O_2 antibonding orbitals.[43,44] As a matter of fact, the polarization of the C−N bond as well as the net atomic electronic charge distribution on selected N-containing heterocycles can be invoked as a descriptor for the catalyst/substrate interaction, proviso that a fine-tuning of the N-dopants in the carbon nanostructures can be achieved.

For the sake of clearness, a certain role of the metallic impurities (catalyst traces) on the electrochemical performance of the commonly prepared N-CNMs cannot be definitively ruled out.[45,46] Anyway, the chemical approach described hereafter to the CNT N-decoration, the direct comparison with the electrochemical behavior of the pristine CNMs, and the nonstructurally invasive character of the adopted functionalization protocol strengthen the hypothesis of an entirely metal-free process at work.

The type of nitrogen functional groups and the nitrogen doping level strongly depend on the applied synthetic conditions;[6−10,47−50] a precise control of these factors still remains far from being exhaustively accomplished. If a partial

control on the degree and type of N-doping in 1D N-CNMs is achieved through an accurate optimization of the CVD synthetic conditions,[51,52] a similar goal seems to be more efficiently approached in the case of 2D N-CNMs through the annealing of undoped CNMs in the presence of well-defined N-containing precursors.[53] Irrespective of the method used, different N-functionalities (such as pyridinic N, pyrrolic N, quaternary N, etc..) often coexist in the as-synthesized N-CNMs; a simple adjustment of their relative concentration in the material remains the only tunable parameter. As a consequence, the role of the different N-functionalities on the catalytic efficiency of the as-synthesized N-CNMs still remains rather elusive and it is at the origin of controversial debates in the scientific community, sometimes producing even conflicting literature results.[6−10,53]

Wågberg and co-workers have recently demonstrated how a thermal postsynthetic treatment on CVD-prepared N-doped MWCNTs can result in the transformation of pyrrolic and pyridinic nitrogen sites into quaternary nitrogen sites (N-Qs), with an overall improvement of the electrocatalytic performance in the ORR.[54,55] Although any conclusion on the electrocatalytic contribution of pyridinic and quaternary N-functionalities still remains difficult to draw up,[56−65] and the role of the total N-loading on the ORR activity looks rather uncertain,[66−69] it is accepted that nitrogen sites located at the graphitic edge planes[54,55,66] exhibit the highest catalytic efficiency in ORR. Accordingly, a $4e^-$ reduction path takes place prevalently on the nitrogen *edge* defects [i.e., on the pyridinic and on the quaternary N-sites (the so-called "valley graphitic-N")], while a less efficient $2e^-$ process preferentially occurs on the *in-plane* nitrogen defects.[70]

Taking advantage of these fundamental concepts, chemical functionalization represents a valuable and alternative approach to the nitrogen decoration of complex carbon nanostructures by means of tailored "edge-type" N-containing functionalities.[71] Compared with the classical CVD approach, chemical functionalization offers a unique tool for the rationalization of the fundamental structure−reactivity relationship of N-doped carbon nanomaterials active in the ORR. Moreover, it lists a number of remarkable technical advantages: (i) the energy-saving conditions required for the CNT decoration with well-defined N-containing functional groups; (ii) their easy chemical and structural tuning; (iii) a substantial atom-economy decoration strategy (full exposure of the N-containing groups to the nanomaterial outer side where the catalytic reaction takes place); (iv) a remarkable electrocatalytic activity and long-term stability of the as-prepared N-doped carbon nanostructure employed as metal-free systems for the ORR in a basic environment. In a preliminary study,[71] some of us have demonstrated how simple pyridine groups embedded in a conjugated (although spatially limited) sp^2 carbon network and covalently linked to the CNT sidewalls can guarantee remarkable catalytic performance in the ORR, in terms of both onset potential (E_{on}) and diffusion-limited current density (J) values. The interest for tailored electron-poor N-containing groups as mimics of "nitrogen edge-type defects" stems from their postulated ability to improve the onset potential values in the electrochemical mediated ORRs.[53] Here we report a full account of the synthesis, characterization, and electrocatalytic activity of a series of MWCNTs functionalized with a variety of well-defined pyridine groups. This study highlights the central role played by the pyridine moiety on the electrocatalytic activity of these N-decorated MWCNTs in the ORR. Most

importantly, clear-cut evidence of the role of the electronic charge density distribution at the chemically grafted N-heterocycles on the final catalyst performance in the ORR is given. Such a result introduces an additional level of complexity to the rationalization and comprehension of the ultimate role of the pyridine groups on the electrocatalytic performance in the ORR promoted by these nanomaterials.

■ EXPERIMENTAL SECTION

General Considerations. All manipulations were carried out under dry nitrogen atmosphere using standard Schlenk-type techniques. Nitrogen (>99.999%; Rivoira) was dried through a $CaCl_2$ column and deoxygenated with an oxysorb cartridge from Messer Griesheim prior to use. oDCB (o-dichlorobenzene) was dried according to the literature procedures[72] and stored under nitrogen atmosphere. Dry acetonitrile (CH_3CN) was obtained by means of an MBraun Solvent Purification System. MWCNTs (98% in C) were purchased from Sigma-Aldrich (lot. no. MKBH5814 V) and used as received. Unless otherwise stated, all other chemicals were purchased from commercial suppliers and used as received without further purification. Sample sonication was carried out using an Elma S15 Elmasonic sonicator bath (37 kHz) while cooling the samples in a water/ice mixture throughout the treatment. CNT filtration was accomplished by using inorganic PTFE filters (Whatman) with 0.2 μm pore size. All measurements carried out on pristine MWCNTs and functionalized samples (MW@N_{1-6}) were conducted on samples which underwent identical washing/filtration/sonication/work-up procedures. For each functionalized sample (MW@N_{1-6}), a "blank functionalization test" was performed using identical reaction conditions and reagents except for the use of the isopentyl nitrite reagent. RRDE measurements on the blank samples have excluded any electrochemical activity associated with potentially physisorbed N-containing heterocycles.[71] Furthermore, any electrochemical activity (RRDE measurements) potentially associated with reagent and solvent contaminations has been properly ruled out using a blank test conducted on MWCNTs treated with the isopentyl nitrite in oDCB/CH_3CN mixture.

General Procedure for the ex Situ MWCNT Functionalization via Aryldiazonium Salt Chemistry. In a typical procedure, MWCNTs (40 mg) were weighed into a two-necked 100 mL flask and suspended in 32 mL of dry and degassed oDCB. The suspension was sonicated for 30 min and then treated with a degassed acetonitrile solution (16 mL) of the corresponding aniline (0.86 mmol). Isopentyl nitrite (0.17 mL, 1.30 mmol) was added via syringe, and the suspension was further sonicated for 10 min. The mixture was heated at 80 °C for 14 h under stirring and nitrogen atmosphere. Afterward the mixture was cooled to room temperature, diluted with ethyl acetate (20 mL), and sonicated for 20 min before being centrifuged to recover the solid residue. The latter was then washed with ethyl acetate and then twice with dichloromethane, each time sonicated for 10 min and separated from the supernatant by centrifugation. The solid residue was finally suspended in dichloromethane, sonicated for 20 min, and filtered through a 0.2 μm pore PTFE filter. The collected material was dried at 50 °C under vacuum to constant weight and stored on air at room temperature.

Material Characterization and Analyses Conditions. *Thermogravimetric Analyses (TGA).* Analyses were performed under air (100 mL/min) on an EXSTAR Thermo Gravimetric Analyzer (TG/DTA) Seiko 6200.

X-ray Photoelectron Spectroscopy (XPS). Analyses were performed with a Thermo Fisher Theta Probe spectrometer equipped with a monochromatic Al Kα X-ray source (1486.6 eV) with a spot size of 300 μm, corresponding to a power of 70 W and at a takeoff angle of 53° relative to the sample normal. Samples in the form of powders were fixed on ultrahigh vacuum compatible Cu adhesive tape (3M) ensuring, as much as possible, an uniform coverage.

Survey spectra (0−1300 eV) were acquired at a pass energy of 200 eV with an energy step size of 1 eV. High resolution spectra were recorded at a pass energy of 100 eV with a step size of 0.05 eV. In the

set conditions the overall energy resolution was 0.9 eV. When needed, charge compensation for treated MWCNTs was accomplished by a low energy electron flood gun (1 eV). Charge correction of the spectra was performed by taking the sp^2 graphitic component of the C 1s spectrum as internal reference (binding energy, BE = 284.6 eV). Special care was devoted during the analyses, to verify that no change in the samples was induced by exposure to the X-ray beam and the electron flood gun. XPS analysis was repeated on three different spots for each sample. High resolution spectra of detected elements were acquired for quantitative and detailed BE chemical shift analysis. Atomic percentages were calculated using the Scofield sensitivity factors set in the Thermo Avantage V4.87 software (Thermo Fisher Corporation) and a nonlinear Shirley background subtraction algorithm. The high resolution spectra were fitted with mixed Gaussian−Lorentzian peaks after a Shirley background subtraction. The determined standard deviation in the peak position was ±0.2 eV.

Raman Spectra. Spectra were recorded using a LabRAM ARAMIS Horiba Raman spectrometer equipped with a 1200 grooves/mm grating and recorded by a Peltier-cooled CCD detector. Spectra were recorded over the range of 200−3200 cm^{-1} using the 532 nm emission of a YAG laser source with laser quantum MPC600 PSU. The beam profile was cleaned by a spatial filter, and Rayleigh scattering was filtered out using EDGE filters. The spectral resolution was 1 cm^{-1}. The incident laser power on the sample was lower than 42 mV, and any damage of the sample due to the laser was carefully checked and excluded. Samples were prepared by gently pressing CNTs and MW@N_{1-6} fine powders into a flat thin film on glass substrate, and each sample was recorded randomly on three different positions.

Raman spectroscopy was employed to investigate a change in the structure during the CNT N-decoration by detecting the presence and strength of D and G modes.[73] The Raman spectrum shows a D band at around 1360 cm^{-1}, and a G band at 1590 cm^{-1}, which correspond to the presence of sp^3 defects and tangential vibration of sp^2 carbon atoms in the hexagonal plane of graphite-like structures, respectively. All recorded curves were baseline and fitted using Lorentzian line-shapes, and the D- and G-peak intensities were used for the calculation of the I_D/I_G ratios.[73−75]

Transmission Electron Microscopy (TEM). Analysis of modified and unmodified CNTs was performed by a Philips CM12 microscope operating at 120 kV, on samples prepared by drop-casting previously sonicated suspensions (EtOH) over copper grids coated with a Formvar film (FF200-Cu-Formvar film only). TEM images were recorded with a CCD camera (Gatan 791).

Rotating-Ring Disk Electrode (RRDE). Measurements were performed using a ring-disk electrode from Pine Instrument Co. consisting of a glassy carbon (GC) disk insert (⌀ 5 mm; A = 0.196 cm^2) and a Pt ring (A = 0.11 cm^2) The RRDE measurements were carried out using a modulated speed rotator (MSR) from Pine Instrument Co. All the measurements were carried out using an Autolab potentiostat/galvanostat in a single compartment glass cell using a three-electrode arrangement. The working electrode was prepared as follows: a proper amount of CNTs (10 mg) was dispersed in 0.220 g of water, 0.112 g of ethanol, and 0.084 g of a Nafion solution (5 wt % in lower aliphatic alcohols and water). The resulting ink was sonicated for 30−45 min and drop-casted onto the glassy carbon electrode (3 mg). The as-prepared electrode was then dried at room temperature. A platinum wire was used as counter electrode, and a double junction Ag/AgCl/KCl sat. electrode served as reference electrode. All CV and RRDE experiments were carried out at a scan rate of 5 mV/s in the potential range from −1.1 to +0.2 V vs Ag/AgCl/KCl sat. Nitrogen or oxygen was used to purge the solution to achieve an oxygen-free or an oxygen-saturated electrolyte solution, respectively. Commercial Metrohm Pt electrode (⌀ 3 mm) was used for comparison, and all measurements were repeated at least four times. Finally, the measurement setup, the moderate electrolyte viscosity, and the entity of the measured currents did not require any ohmic compensation.

All prepared CNT inks were indefinitely stable in air for months with neither any apparent decomposition nor alteration of their electrochemical performance. The number of electrons transferred per

3462

dx.doi.org/10.1021/cm500805c | *Chem. Mater.* 2014, 26, 3460−3470

O_2 molecule (n) in the ORR for the different catalysts has been calculated by the Koutecky–Levich equation applied to the ORR curves obtained at different rotation rates (rpm).[76] The Koutecky–Levich is given by the following equation:

$$\frac{1}{j} = \frac{1}{j_{cc}} + \frac{1}{nK_f\sqrt{f}} \quad \text{with} \quad K_f = 0.2FC_0D_0^{2/3}\nu^{-1/6} \tag{1}$$

where j is the current density, j_{cc} is the kinetic current density, n is the number of exchanged electrons, F is the Faraday constant, D_0 is the oxygen diffusion coefficient (1.95×10^{-5} cm^2 s^{-1}), f is the angular rotation rate of the electrode (rpm), ν is the kinematic viscosity of the solution (0.008977 cm^2 s^{-1}), and C_0 is the O_2 concentration in solution (1.15×10^{-3} mol dm^{-3}).[13] With these parameters, the value of K_f constant is 0.03538. The average number of electrons (n) exchanged during the ORR has been extrapolated from the slop of the plot of j^{-1} versus $f^{-1/2}$ at a specific potential value. We have recorded the voltammetric curves from −1.1 to 0.2 V at different rotation rates (from 400 to 2000 rpm) and calculated the n values in the diffusion and kinetically limited regions (from −0.65 to −0.95 V).

Elemental analyses were performed using a Thermo FlashEA 1112 Series CHNS-O elemental analyzer, and elemental average values were calculated over three independent runs.

Acid–Base Titration of N-CNMs MW@N$_{1–6}$. Five milligrams of the selected N-decorated material (MW@N$_{1–6}$) were suspended in 7 mL of a standard HCl solution (2.8×10^{-3} M, standardized with Na_2CO_3 as primary standard), sonicated for 30 min, and maintained in the dark at rt under stirring for 48 h. Afterward the suspension was centrifugated, and three aliquots of the supernatant solution were titrated with a standardized solution of NaOH (2×10^{-3} M). The pyridine content (N$_{Py}$%) was calculated for each sample as the average value over the three independent runs.[77,78]

Computational Details. Density functional theory (DFT) calculations were performed in the gas phase using the Gaussian09 program (revision C.01).[79] The real structures of the dangling groups on the CNTs were optimized with a B3LYP functional[80] using a 6-31G** basis set on all atoms. A Grimme D3 dispersion correction was also included in the optimization, through the Gaussian IOp(3/124 = 30) keyword.[81] Bader charge partitioning was made through the free algorithm developed at Texas University available at http://theory.cm.utexas.edu/bader/. The Gaussian *.cube file coming from the optimizations was taken as the starting point for the Bader analysis on a charge density grid.[82]
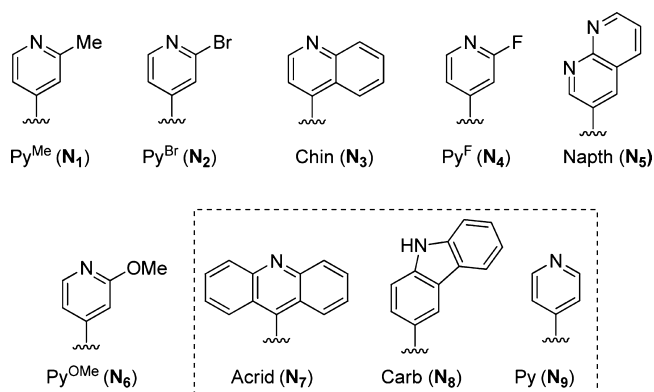
■ RESULTS AND DISCUSSION

The main objective of the present study is to provide a clear-cut understanding of the complex structure–reactivity relationship which drives the electrocatalytic performance of carbon nanomaterials decorated with well-defined N-containing functionalities (i.e., pyridinic-N sites). Besides offering a definitive answer to the widely debated question dealing with the role played by pyridine groups on the electrocatalytic activity of N-functionalized/doped carbon nanomaterials in the ORR, the obtained results suggest the existence of a coherent descriptor of the catalyst performance (at least in terms of onset potential values) based on the electronic charge density distribution at the N-neighboring carbon atoms as well as on the related N–C$_\alpha$ bond polarization.

On a merely speculative ground, the concept of "doping" is more properly referred to those CNMs featured by "implanted" heteroelements in the sp^2 carbon network; therefore, it should be kept distinguished from that of "chemical functionalization" with heteroelement-containing functionalities attached to the carbon basal or edge planes. On the other hand, selected "dopants" or "heterofunctionalities", like those containing pyridine or pyrrole groups, are conceivable as "edge-type" groups only, and therefore "chemical functionalization" can be

proposed as a valuable alternative path to bring N-containing functionalities on the CNM's board as edge-type defect mimics. Such an approach offers a unique tool for the unambiguous understanding of the catalytic role exerted by selected N-containing groups in the ORR, paving the way to the development of tailored and more catalytically active metal-free electrocatalysts for the ORR and providing a simplified model for the in-depth understanding of the underlying reaction mechanisms.

Following our preliminary studies on acridine- and pyridine-functionalized MWCNTs,[71] a series of variably substituted pyridine groups have been selected as candidates for the chemical functionalization of MWCNTs (Scheme 1).

**Scheme 1. N-Containing Heterocycles Used for the MWCNT Decoration (N$_{1–6}$ this work)^a**

Py^{Me} (N$_1$)   Py^{Br} (N$_2$)   Chin (N$_3$)   Py^F (N$_4$)   Napht (N$_5$)

Py^{OMe} (N$_6$)   Acrid (N$_7$)   Carb (N$_8$)   Py (N$_9$)

^{a}Functional groups N$_{7–9}$ (included in the dashed frame) have already been discussed elsewhere[71] and cited here for completeness.

A control on the electronic properties of the heterocycles as well as on the polarization of the N–C$_\alpha$ bond is made possible through a selection of either electron-donating (EDG) or electron-withdrawing (EWG) groups attached to the α-position of the pyridine ring.

Synthesis and Characterization of the N-Functionalized MW@N$_{1–6}$ Samples. The adopted procedure for the N-decoration of the MWCNTs is based on the classical aryldiazonium salt chemistry (Tour protocol).[83–90] The functionalization is conveniently performed under relatively mild reaction conditions (Scheme 2), starting from pristine MWCNTs and one aniline derivative chosen among the selected N-containing moieties (Scheme 1).

Each functionalized sample undergoes a careful work-up procedure made of successive and multiple sonication/centrifugation and filtration cycles as to remove all the

Scheme 2. MWCNT N-Decoration via Aryldiazonium Salt (Tour) Protocol (MW@N$_{1–6}$ in this work)^a
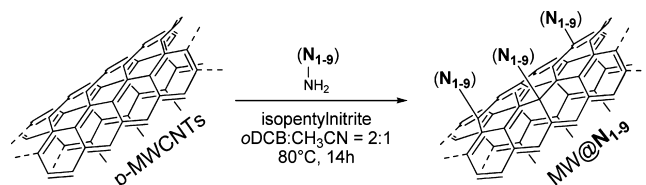
^{a}Samples MW@N$_{7–9}$ have been already discussed elsewhere[71] and cited here for completeness.
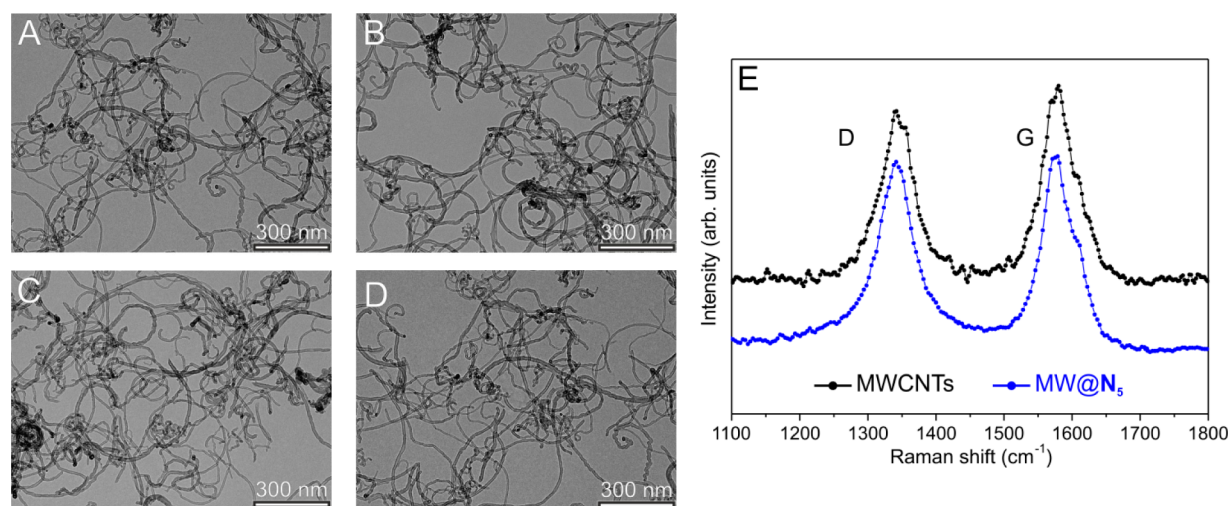
Figure 1. (left) TEM images of pristine MWCNTs (A) and MW@N_2 (B), MW@N_3 (C), MW@N_4 (D) samples. (right) Raman spectra of pristine MWCNTs (black) and MW@N_5 (blue) as representative samples. For all other Raman spectra and relative fitting curves, see Figure S1, Supporting Information.

Table 1. Calculation of the N-Functional Loading on Each MW@N Sample

	elemental analysis[a]			acid−base titration[b]	XPS analysis
	C (%)	N (%)	N (wt %)[c] ; [mmol g^{-1}][d]	N_{Py} (wt %) ; [mmol g^{-1}][d]	N (at. %) ; [mmol g^{-1}][f]
p-MWCNTs[e]	93.83	0.20			
MW@N_1	90.58	1.22	1.02 ; [0.73]	0.89 ; [0.64]	1.9 ; [1.50]
p-MWCNTs[e]	93.97	0.09			
MW@N_2	92.65	0.51	0.42 ; [0.30]	0.35 ; [0.25]	0.6 ; [0.48]
p-MWCNTs[e]	95.30	0.17			
MW@N_3	90.97	1.45	1.28 ; [0.91]	1.21 ; [0.86]	1.5 ; [1.13]
p-MWCNTs[e]	95.04	0.03			
MW@N_4	92.05	0.44	0.41 ; [0.29]	0.26 ; [0.19]	0.6 ; [0.49]
p-MWCNTs[e]	92.75	0.33			
MW@N_5	91.34	1.98	1.65 ; [1.18]	1.47 ; [1.05]	2.0 ; [1.54]
p-MWCNTs[e]	95.30	0.02			
MW@N_6	91.99	0.74	0.72 ; [0.51]	0.76 ; [0.54]	1.1 ; [0.85]

[a]Average C% and N% values calculated over three independent runs. [b]Average N_{Py}% values calculated over three independent runs. [c]The N% content calculated as difference between the N-content (%) of each functionalized sample (MW@$N_{1−6}$) and the respective "blank sample" (p-MWCNTs). [d]Relative functional group loading. [e]"Blank samples" prepared using identical reaction conditions, reagents, and work-up procedure applied to the synthesis of MW@$N_{1−6}$ samples, except for the use of the isopentyl nitrite as reagent. [f]Relative functional group loading calculated from the extrapolated N (wt %).

unreacted reagents. A blank functionalization test (a parallel reaction conducted in the absence of the isopentyl nitrite reagent) is carried out for each aniline sample, with the aim of quantifying the residual amount (traces) of physisorbed N-contaminants potentially derived from the reaction procedure. All the as-prepared samples (MW@$N_{1−6}$) have been spectroscopically (XPS, Raman) and morphologically (TEM) characterized. In the TEM analyses, all the functionalized materials (MW@$N_{1−6}$) do not present any appreciable morphological change in terms of either tube length and diameter or bundle aggregation on the whole scanned area. Figure 1B−D shows TEM pictures recorded on a selection of the most representative functionalized samples (Figure 1B: MW@N_2; Figure 1C: MW@N_3; Figure 1D: MW@N_4) compared with the pristine ones (Figure 1A). Similarly, Raman spectra of all the MW@N samples do not reveal any major change in the intensity ratio of the D and G modes (I_D/I_G), this parameter being commonly used as a benchmark of the crystallite and defect site surface density alteration (Figure 1E

and Figure S1, Supporting Information). The Raman and TEM issues are consistent with a noninvasive N-decoration procedure which leaves the main physicochemical properties of the functionalized materials unchanged while grafting tailored pyridine-based dangling groups to their outer surface. A preliminary evidence of the occurred functionalization is given by the analysis of the thermogravimetric profiles (TGA). All samples are heated in air within the same temperature range (40−900 °C); a more gradual decomposition profile is evidenced for all the N-decorated samples when compared with the pristine ones (Figure S2, Supporting Information). Such a trend, indicative of a slightly increased "sidewall roughness" as a consequence of the functionalization procedure, does not give more than a qualitative indication of the occurred CNTs decoration. A quantitative loading of the N-containing heterocycles is provided by the crossed comparison of the CHN elemental analysis and the acid−base titration of the pyridinic basic sites (Table 1). The acid−base titration guarantees the most reliable and accurate quantification of the

N-loading, restricting the measurement to those N-containing groups really available and/or chemically accessible at the CNT surface (see also Table S1, Supporting Information).

As Table 1 shows, elemental analysis provides N-contents for almost all the functionalized samples with slight overloadings (compared to the acid−base titration) ranging from 0.07 to 0.18 N%. The lower functionalization loading measured for materials containing pyridine functionalities substituted with inductive EWGs (samples MW@N$_2$, MW@N$_4$, MW@N$_6$) is in line with the electron-poor character of these heterocycles and their subsequent ability to stabilize the postulated reactive aryl radical intermediates during the Tour reaction protocol.[91]

XPS spectra of MW@N$_{1−6}$ show characteristic N 1s profiles featured by one main peak in the 398.8−399.3 eV range, consistent with the presence of pyridine nuclei (Figure 2).[51,92]

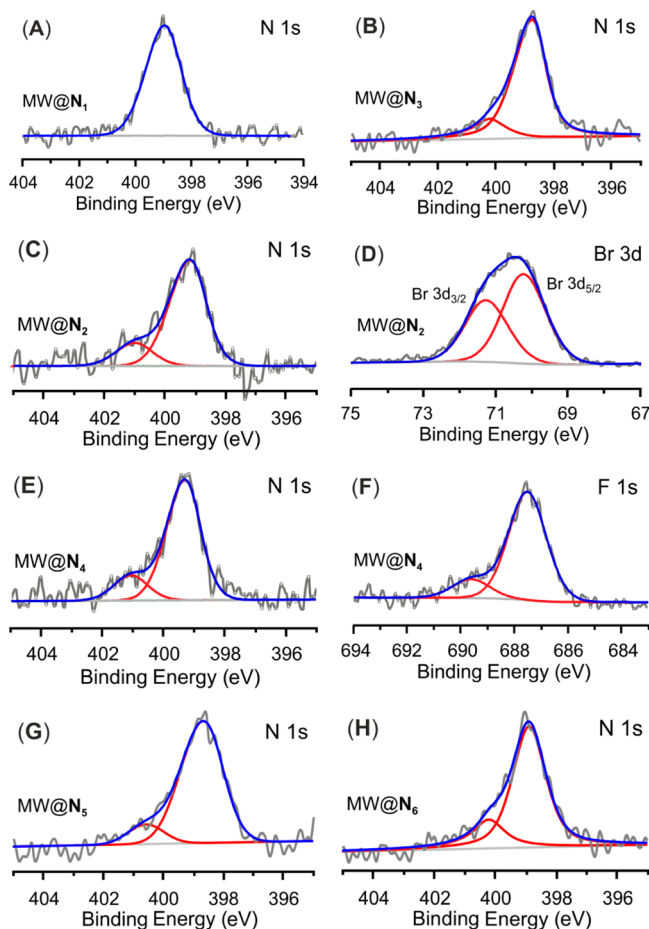

Figure 2. High resolution N 1s (A: MW@N$_1$; B: MW@N$_3$; C: MW@ N$_2$; E: MW@N$_4$; G: MW@N$_5$; H: MW@N$_6$), Br 3d (D: MW@N$_2$), and F 1s (F: MW@N$_4$) core level regions and their relative fits for the XPS spectra of samples MW@N$_{1−6}$.

Although not catalytically relevant (see Experimental Section), minor residues coming from solvents and/or reagents retained by the material porosity are not totally removed by the work-up procedure. Accordingly, minor N 1s shoulders at higher binding energy values and present in almost all functionalized samples (Figure 2B,C,E,G,H) are ascribed to commonly observed surface contaminations.[71,93] Figure 2D shows the typical Br 3d signal consisting of a doublet (Br 3d$_{5/2}$ and Br 3d$_{3/2}$, respectively, at 70.7 and 71.8 eV) due to spin−orbit coupling,[94] the position being indicative of a Br-pyridine group.

A little shoulder at higher binding energy values in the F 1s spectrum of MW@N$_4$ has been explained by invoking two different fluorine environments (Figure 2F); the main peak at 687.4 eV (85%) is ascribed to the 2-fluoropyridine moiety, while the minor component at 689.6 eV (15%) is indicative of a direct binding of F to the MWCNT sidewall.[91]

From a quantitative point of view, the overall N-loading measured through XPS is typically much closer to the elemental analysis values than those coming from the acid−base titration (Table 1). Apart from slightly overestimated N-loadings, the XPS technique provides unambiguous evidence of the surface material decoration with the expected N-containing heterocycles.

Electrochemical Tests on MW@N$_{1−6}$ Samples as Electrocatalysts for the ORR. After the material characterization, the study of their electrocatalytic performance in the ORR has been performed. To this purpose, a MW@N/Nafion ink is prepared for each functionalized sample and subsequently casted on a rotating glassy carbon (GC) electrode to give a thin and homogeneous film after solvent evaporation (see Experimental Section). The as-prepared electrocatalysts have been investigated by cyclic voltammetry (CV) using a three-electrode cell consisting of an Ag/AgCl/KCl saturated reference electrode and a Pt counter electrode operating in a 0.1 M KOH solution.

As Figure 3 shows, under O$_2$-saturated conditions each N-decorated sample presents a well-defined ORR cathodic peak not present under a saturated N$_2$ environment. To gain further insights into the oxygen reduction reaction, rotating ring disk electrode (RRDE) voltammograms are acquired in O$_2$-saturated 0.1 M KOH electrolyte solution and compared with the electrocatalytic performance of the pristine MWCNTs, the bare GC, and a commercial Metrohm Pt-polycrystalline electrode (Ø 3 mm). For all CNMs, the amount of the deposited catalyst is fixed to 358 μg/cm^2 irrespective of the different N-loadings measured on the relative MW@N$_{1−6}$ samples; such a value is assumed in accord with the highest number of exchanged electrons at variable N-CNM ink loadings (see also Table S2, Supporting Information), measured for one of the best performing systems of this series (MW@N$_2$). Linear sweep voltammograms are first recorded for each sample at different spin rates (from 400 to 2000 rpm), while sweeping potentials are recorded linearly from −1.1 to 0.2 V and reversing them against Ag/AgCl/KCl sat. (Figure S3, Supporting Information); for all the electrochemical profiles, background currents measured under saturated N$_2$ conditions at the same potential scan rate (5 mV s$^{−1}$) are subtracted from the respective curves to eliminate all the capacitive contributions.

Figure 4A shows the ORR polarization curves recorded at 800 rpm for each system, along with the respective ring current values relative to the oxidation of hydrogen peroxide ions (HO$_2^−$) measured at the Pt-ring electrode held at a potential of 0.50 V (Figure 4A′). As Figure 4A shows, the onset potentials (E_{on}) measured for all N-CNMs are negatively moved from that of Pt, while maintaining a remarkable and positive shift compared to the GC (a) and pristine MWCNTs (b). For the latter two catalysts only, a clear reduction prewave is observed at low overpotentials, followed by a second reduction wave starting around −0.7 V, this being indicative of a prevalent 2e$^−$ reduction path.[10,13,16,20] Accordingly, lower ring currents are measured for all N-decorated samples (Figure 4A′) compared to pristine MWCNTs and GC. This reduced current is
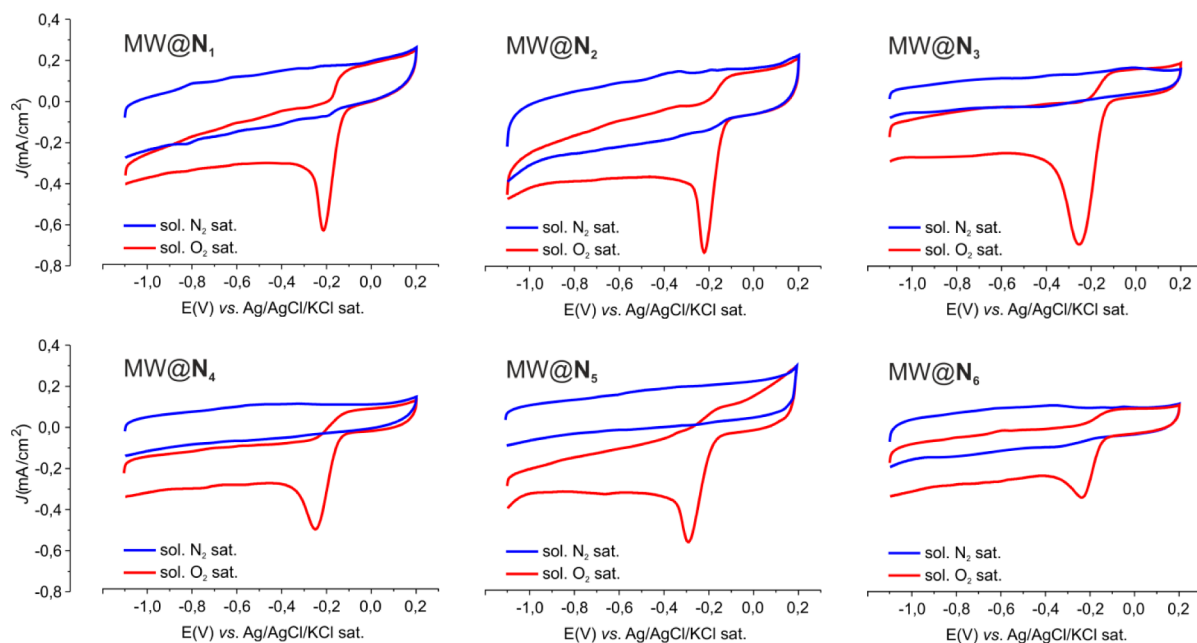
Figure 3. Cyclic voltammograms for MW@N$_{1-6}$ samples recorded under N$_2$-saturated (blue) and O$_2$-saturated solutions (red). The potential was linearly swept from −1.1 to 0.2 V at a scan rate of 5 mV s^{-1} vs Ag/AgCl/KCl sat. as the reference electrode.
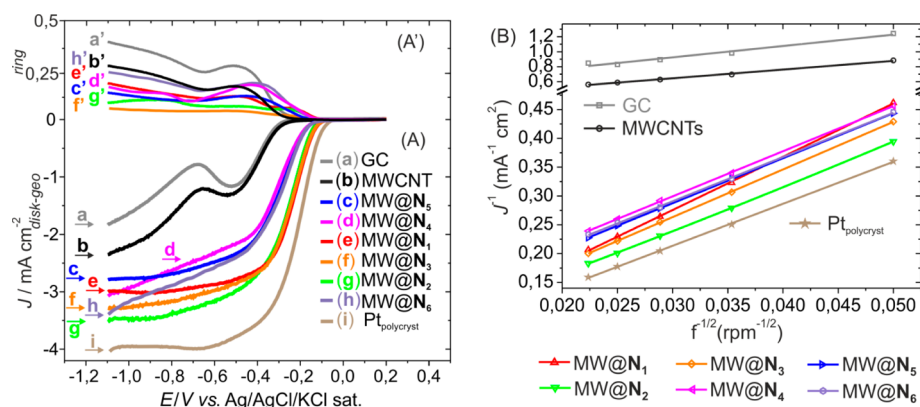

Figure 4. (A) RRDE current−potential curves at 293 K for ORR in O$_2$ saturated 0.1 M KOH solution recorded by using a rotating ring-disk GC electrode [GC disk, $A = 0.196$ cm^2] with (A′) Pt ring [$A = 0.11$ cm^2]. All samples are measured at an angular rotation rate (f) of 800 rpm. (B) K-L plots for MW@N$_{1-6}$, GC, MWCNTs, and Pt catalysts as obtained from the respective LSVs at −0.75 V. Parameters used: O$_2$ concentration (C), 1.15×10^{-3} mol L^{-1}; O$_2$ diffusion coefficient (D), 1.95×10^{-5} cm^2 s^{-1}; kinematic viscosity (ν) of the electrolyte solution, 0.008977 cm^2 s^{-1} (see also the Experimental Section).
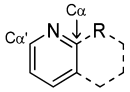
indicative of a decreasing amount of HO$_2^-$ ions reaching the ring electrode under increasing negative potentials. The onset potential (E_{on}) values measured for each catalyst are listed in Table 2. Noteworthy, while ORR starts at −0.299 V (E_{on}) on pristine MWCNTs, corresponding to an overpotential of ca. 200 mV compared to Pt (Table 2, entry 2 vs 9; Figure 4A, b vs i), overpotentials between 34 and 78 mV are measured for all the N-decorated samples. In particular, it is possible to identify two distinct classes of catalysts, each one characterized by similar E_{on} values in the ORR. Among these, the ORR onset potentials measured for MW@N$_1$, MW@N$_2$, and MW@N$_3$ (Table 2, entries 3−5; Figure 4A, curves e, f, g) are shifted to more positive values, thus featuring higher electrocatalytic activity compared to the other N-CNMs. Their ORR performance (number of transferred electrons per O$_2$ molecule) in the diffusion and kinetically limited regions (from −0.65 to −0.95 V) is evaluated on the basis of the Koutecky−Levich (K-L) equation.[13,95] K-L plots of each

Table 2. E_{on} Values (V) and Average Number of Electrons Transferred ($n_{E=-0.75\ V}$) for O$_2$ Molecule As Derived from Plots in Figure 4, Parts A and B, Respectively

entry	catalyst	E_{on} (V)	$n_{E=-0.75\ V}$
1	GC	−0.307	1.9
2	MWCNTs	−0.299	2.5
3	MW@N$_1$	−0.135	3.1
4	MW@N$_2$	−0.144	3.7
5	MW@N$_3$	−0.137	3.4
6	MW@N$_4$	−0.179	3.5
7	MW@N$_5$	−0.168	3.6
8	MW@N$_6$	−0.169	3.5
9	Pt	−0.101	3.9

catalytic system obtained at different potential values (from −0.65 to −0.95 V) are reported in Figure S4, Supporting Information. All curves show excellent linearity, thus implying a

Table 3. Net Bader Charges (q) of the N and C_α Atoms Calculated on N_{1-6} Heterocycles[a]

Entry	N-heterocycle	q_N	$q_{C\alpha}$	$q_{C\alpha'}$	N-C_α bond polarization $[|q_N|+|q_{C\alpha}|]$
1	N_1	-2.857	1.324	1.281	4.181
2	N_2	-2.982	1.504	1.183	4.486
3	N_3	-2.649	1.416	1.258	4.065
4	N_4	-2.905	2.330	1.294	5.235
5	N_5	-2.745	2.649	1.293	5.394
6	N_6	-2.845	2.467	1.208	5.312
7	N_7	-2.696	1.448	1.448	4.144
8	N_8	-2.356	0.828	0.828	3.184
9	N_9	-2.670	1.161	1.161	3.831

[a]Bader analysis of the atomic charge density on previously reported N_{7-9} systems[71] has also been listed here for completeness.

first-order reaction toward dissolved O_2. For the sake of comparison, the K-L plots (J^{-1} vs $f^{-1/2}$) of each catalyst obtained at −0.75 V are reported in Figure 4B. The calculated average number of electrons ($n_{E=-0.75 V}$) transferred per O_2 molecule in the ORR process are outlined in Table 2 (see also the Experimental Section for calculation details).

Notably, the N-functionalized materials show from good to excellent n values measured at −0.75 V for the ORR; this is indicative of a prevailing 4e⁻ reduction process for all these systems. This statement is further supported by the rather moderate ring current values recorded for all N-CNMs at the Pt ring electrode, consistent with a scarce amount of HO_2^- ions produced during the catalytic cycles (Figure 4A').

Compared to the classical preparation protocol (CVD approach), chemical functionalization gives the rare opportunity to rationalize the structure−activity relationship of these metal-free catalysts systematically, through a fine-tuning of the electronic properties of the N-containing heterocycle involved as "active site" in the catalytic process. All the substituted pyridine derivatives used in the study can be roughly conceived as mimics of edge-type N-defects with tunable chemical environment (substituents) that modifies the ring electronic charge density distribution. Most importantly, the functionalization protocol meets the fundamental requirement of maximizing the number of N-edge-sites at the nanomaterial surface, where the oxygen adsorption presents considerably lower energy barriers compared to equivalent undoped edge-sites as well as to in-plane N-sites.[8,30] A comparison between the different N-containing heterocycles present at the CNT sidewalls and the voltammetric performance of the relative MW@N_{1-6} nanomaterials highlights the influence of the electronic charge density distribution at the N-sites (as well as at the N-neighboring carbon atoms) on the ability of the N-CNMs to promote the kinetically sluggish dioxygen reduction reaction more or less efficiently. If electron-accepting nitrogen atoms are known to generate a highly positive charge density on the adjacent C_α atoms, electron-withdrawing (EW) or electron-donating (ED) groups attached to the α-position of the heterocyclic ring certainly have a strong influence on the final atomic charge density redistribution. As a matter of fact, a tuning of the adsorption energy of the dioxygen species (substrate) and/or its reduction intermediates (products) onto the catalytically active sites (N-heterocycle) is expected. In this

regard, we have proposed a rationale to the experimental outcomes in the ORR obtained with the MW@N_{1-6} samples based on the calculation of the Bader atomic charges on each N-heterocycle.[96] After a DFT preoptimization of the dangling substituents (N_1-N_6) at the B3LYP//6-31G** level of theory, a Bader charge analysis has been performed for each case to infer the Bader atomic charges on the N and C_α atoms,[97] whose values are outlined in Table 3.

The analysis of the C_α atomic charges, together with that of the corresponding N−C_α bond polarization, shows a rather well-matching trend with the onset potentials (E_{on}) measured on the respective N-CNMs. An increase of the $q_{C\alpha}$ value translates into the worst E_{on} values (Table 3, entries 4−6, vs Table 2, entries 6−8) while reduced charge densities on the C_α generate a better catalyst performance, at least in terms of E_{on} values (Table 3, entries 1−3, vs Table 2, entries 3−5). Minor discrepancies, as small deviations from the postulated $q_{C\alpha}$ vs E_{on} trend within each of the two series of catalysts (MW@N_{1-3} and MW@N_{4-6}), can be ascribed to the unsymmetrical nature of the N-containing groups. Indeed, a minor contribution from the $C_{\alpha'}$ positions in the catalytic process cannot be definitively ruled out.

In the case of previously reported[71] N-decorated CNMs bearing different N-containing heterocycles [see also Scheme 1, samples N_{7-9} and Table S3 (Supporting Information) for the relative E_{on} values], reduced $q_{C\alpha}$ values [compared to the best performing systems (MW@N_{1-3})] lead to even worse E_{on} values. Such results introduce an additional level of complexity to the original claim that pyridine-like moieties in N-doped CNMs improve the onset potential values of the ORRs.[53] According to our experimental evidence, the nature of the pyridine moieties in N-CNMs plays a fundamental role in favoring a predominant 4e⁻ reduction process, as well as in modulating the overpotential values at which the oxygen reduction starts. Indeed, the variation of the atomic charges on the N-proximal carbon atoms of the heterocycle is strongly linked to the dioxygen adsorption energy on the material "active sites". According to this phenomenological model, an optimal $q_{C\alpha}$ value in the range of 1.32−1.50 (see also Table 3, entries 1−3, 7) is calculated on the samples MW@N_{1-3} and MW@N_7, while N-CNMs showing either higher (MW@N_{4-6}) or lower (MW@N_{8-9}) $q_{C\alpha}$ charges are featured by worse E_{on} performance. Notably, deviations from the optimal $q_{C\alpha}$ values

(Table 3, entries 1−3, 7) can also lead to alternative reduction paths, especially at high overpotentials. This is the case for the samples MW@N_8 (containing pyrrole groups) and MW@N_9 (containing plain pyridine units), where rather moderate $q_{C\alpha}$ values (as well as the relative N−C_α bond polarization values) make a $2e^-$ reduction process highly competitive. In line with this observation, a significant amount of HO_2^- ions is detected during the ORR when using these samples as catalysts. For the two limit samples MW@N_4 and MW@N_6, a diffusion and kinetically limited process (at high overpotentials) seems to be significantly affected by the too high $q_{C\alpha}$ values (see Figure 4A, curves d and h). If any possible rationale to this behavior remains merely speculative, this experimental outcome can be tentatively justified by the presence of an "overcharge" at the C_α that makes the interaction with the reduction intermediates/products too strong for the reaction to proceed further; from this point of view, it can be seen as a sort of "catalyst poisoning". Despite these data, no further discussion can be made on the way dioxygen adsorbs to the "active sites" (side-on mode, also known as the Yeager model, and/or end-on mode, known as the Pauling model)[98] which is another largely debated issue on both an experimental and a theoretical ground. On the other hand, it seems generally accepted that zigzag edge structures (as our chemically grafted N-moieties can be considered) promote a preferential dioxygen end-on adsorption mode.[30]

CONCLUSIONS

MWCNTs decorated with tailored pyridine-containing groups are valuable materials to be used as ORR catalysts giving, at the same time, a unique perspective on some specific structure−reactivity relationship of these metal-free systems. In this study, a number of variably substituted pyridine moieties are brought on the CNT board (basal or edge planes) through a well consolidated chemical functionalization approach. If it is accepted that pyridine nuclei in N-CNMs play an important role in the improvement of the overpotential values at which the oxygen reduction starts,[53] a control of their electronic properties through inductive electron-donating (EDG) or electron-withdrawing (EWG) groups attached to the α-position of the pyridine ring adds another level of complexity to the rationalization of the electrochemical outcomes. Indeed, variations of the atomic charges on the α-carbon atoms of the heterocycles (as well as the related N−C_α bond polarization) translate into systems featured by different E_{on} values. One possible rationale to this phenomenological trend is attributed to the change of the adsorption energy of the dioxygen species (substrate) and/or its reduction intermediates (products) onto the catalytically active sites (N-heterocycle). The calculation of the Bader atomic charges on each substituted heterocycle has been used to rationalize the observed electrochemical trend. As a result, MW@N featured by the best onset potentials (E_{on} ranging from 0.135 to 0.144 V) are associated with $q_{C\alpha}$ values measured in the 1.32−1.50 range (and the respective N−C_α bond polarization values in the 4.0−4.5 range). Out of this range, higher or lower $q_{C\alpha}$ charges (or N−C_α bond polarization values) translate into catalytic systems showing worse E_{on} performance. In addition, the electrochemical results reveal how deviations from the optimal $q_{C\alpha}$ values can trigger alternative reduction paths, especially at high overpotentials.

Overall, the results outlined in the paper demonstrate that pyridine-functionalized MWCNTs generate valuable electro-

catalysts for the ORR. This alternative approach to the heterodecoration of carbon nanomaterials stress the importance of the N-chemical surrounding on the catalytic performance of the N-functionalities, offering both an excellent work basis to the development of more catalytically active metal-free electrocatalysts for the ORR and an unique model for the in-depth understanding of the underlying ORR mechanism.

ASSOCIATED CONTENT

S Supporting Information

Raman spectra, TGA profiles, acid−base titration details, and electrochemical data processing for samples MW@N_{1-6} (PDF). This material is available free of charge via the Internet at http://pubs.acs.org.

AUTHOR INFORMATION

Corresponding Author

*Fax: +39 055 5225203. E-mail: giuliano.giambastiani@iccom.cnr.it.

Notes

The authors declare no competing financial interest.

ACKNOWLEDGMENTS

REFERENCES

(1) Antolini, E. *Appl. Catal., B* **2009**, *88*, 1−24.
(2) Shao, Y.; Yin, G.; Gao, Y. *J. Power Sources* **2007**, *171*, 558−566.
(3) Borup, R.; Meyers, J.; Pivovar, B.; Kim, Y. S.; Mukundan, R.; Garland, N.; Myers, D.; Wilson, M.; Garzon, F.; Wood, D.; Zelenay, P.; More, K.; Stroh, K.; Zawodzinski, T.; Boncella, J.; McGrath, J. E.; Inaba, M.; Miyatake, K.; Hori, M.; Ota, K.; Ogumi, Z.; Miyata, S.; Nishikata, A.; Siroma, Z.; Uchimoto, Y.; Yasuda, K.; Kimijima, K.-I.; Iwashita, N. *Chem. Rev.* **2007**, *107*, 3904−3951.
(4) Zhang, S.; Yuan, X.; Wang, H.; Mérida, W.; Zhu, H.; Shen, J.; Wu, S.; Zhang, J. *Int. J. Hydrogen Energy* **2009**, *34*, 388−404.
(5) Morozan, A.; Jousselme, B.; Palacin, S. *Energy Environ. Sci.* **2011**, *4*, 1238−1254.
(6) For a critical review article on the topic, see: Zheng, Y.; Jiao, Y.; Jaroniec, M.; Jin, Y. G.; Qiao, S. Z. *Small* **2012**, *8*, 3550−3566 (see also refs 7−10).
(7) Zhu, C. Z.; Dong, S. J. *Nanoscale* **2013**, *5*, 1753−1767.
(8) Wang, D.-W.; Su, D. *Energy Environ. Sci.* **2014**, *7*, 576−591.
(9) Yu, D.; Nagelli, E.; Du, F.; Dai, L. *J. Phys. Chem. Lett.* **2010**, *1*, 2165−2173.
(10) Song, C.; Zhang, J. Electrocatalytic Oxygen Reduction Reaction. In *PEM Fuel Cell Electrocatalysts and Catalyst Layers: Fundamentals and Applications*; Zhang, J., Ed.; Springer: New York, 2008; pp 89−134.
(11) ORRs based on metal-free or non-noble metal catalystsin acidic media are generally more critical. To the best of our knowledge, only Pt and its alloys show the best ORR activity in acidic electrolytes: see Li, Y. G.; Zhou, W.; Wang, H. L.; Xie, L. M.; Liang, Y. Y.; Wei, F.; Idrobo, J. C.; Pennycook, S. J.; Dai, H. J. *Nat. Nanotechnol.* **2012**, *7*, 394−400.
(12) Kinetics for ORRs in alkaline electrolyte are more favored compared to those performed in acidic media, due to the lower overpotential associated with the first electron transfer to the O_2 adsorbed at the catalyst surface ($_{ad}O_2 \rightarrow {}_{ad}O_2^{\bullet-}$; 0.7 V at pH = 14 vs 1.53 V at pH = 0): see Blizanac, B. B.; Ross, P. N.; Markovic, N. M. *Electrochim. Acta* **2007**, *52*, 2264−2271.
(13) Wang, Y.; Zhang, D.; Liu, H. *J. Power Sources* **2010**, *195*, 3135−3139.
(14) Zhang, M. *Langmuir* **2004**, *20*, 8781−8785.

(15) Su, D. S.; Zhang, J.; Frank, B.; Thomas, A.; Wang, X.; Paraknowitsch, J.; Schlögl, R. *ChemSusChem* **2010**, *3*, 169−180.

(16) Kruusenberg, I.; Leis, J.; Arulepp, M.; Tammeveski, K. *J. Solid State Electrochem.* **2010**, *14*, 1269−1277.

(17) Jin, H.; Zhang, H.; Zhong, H.; Zhang, J. *Energy Environ. Sci.* **2011**, *4*, 3389−3394.

(18) Gong, K.; Du, F.; Xia, Z.; Durstock, M.; Dai, L. *Science* **2009**, *323*, 760−764 and refs 19−25.

(19) Chizari, K.; Deneuve, A.; Ersen, O.; Florea, I.; Liu, Y.; Edouard, D.; Janowska, I.; Begin, D.; Pham-Huu, C. *ChemSusChem* **2012**, *5*, 102−108.

(20) Morozan, A.; Jégou, P.; Pinault, M.; Campidelli, S.; Jousselme, B.; Palacin, S. *ChemSusChem* **2012**, *5*, 647−651.

(21) Geng, D.; Chen, Y.; Chen, Y.; Li, Y.; Li, R.; Sun, X.; Ye, S.; Knights, S. *Energy Environ. Sci.* **2011**, *4*, 760−764.

(22) Parvez, K.; Yang, S.; Hernandez, Y.; Winter, A.; Turchanin, A.; Feng, X.; Müllen, K. *ACS Nano* **2012**, *6*, 9541−9550.

(23) Unni, S. M.; Devulapally, S.; Karjule, N.; Kurungot, S. *J. Mater. Chem.* **2012**, *22*, 23506−23513.

(24) Qu, L.; Liu, Y.; Baek, J.-B.; Dai, L. *ACS Nano* **2010**, *4*, 1321−1326.

(25) Rao, C. V.; Ishikawa, Y. *J. Phys. Chem. C* **2012**, *116*, 4340−4346 See also refs 3d and 4a.

(26) Yeh, K.-Y.; Janik, M. J. *J. Comput. Chem.* **2011**, *32*, 3399−3408.

(27) Yu, L.; Pan, X.; Cao, X.; Hu, P.; Bao, X. *J. Catal.* **2011**, *282*, 183−190.

(28) Kaukonen, M.; Krasheninnikov, A. V.; Kauppinen, E.; Nieminen, R. M. *ACS Catal.* **2013**, *3*, 159−165.

(29) Ni, S.; Li, Z.; Yang, J. *Nanoscale* **2012**, *4*, 1184−1189.

(30) Kim, H.; Lee, K.; Woo, S. I.; Jung, Y. *Phys. Chem. Chem. Phys.* **2011**, *13*, 17505−17510.

(31) Guldi, D. M.; Martin, N. *Carbon Nanotubes and Related Structures Synthesis, Characterization, Functionalization, and Applications*; Wiley-VCH: Weinheim, 2010. Zhang, Y.; Zhang, L.; Zhou, C. *Acc. Chem. Res.* **2013**, *46*, 2329−2339.

(32) Zhang, Y.; Zhang, L.; Zhou, C. *Acc. Chem. Res.* **2013**, *46*, 2329−2339.

(33) Higgins, C. D.; Wu, J.; Li, W.; Chen, Z. *Electrochim. Acta* **2012**, *59*, 8−13.

(34) Unni, S. M.; Devulapally, S.; Karjulea, N.; Kurungot, S. *J. Mater. Chem.* **2012**, *22*, 23506−23513.

(35) Yang, H.; Shan, C.; Li, F.; Han, D.; Zhang, Q.; Niu, L. *Chem. Commun.* **2009**, 3880−3882.

(36) Park, S.; Hu, Y.; Hwang, Y. O.; Lee, S. E.; Casabianca, L. B.; Cai, W.; Potts, J. R.; Ha, H. W.; Chen, S.; Oh, J.; Kim, S. O.; Kim, Y. H.; Ishii, Y.; Ruoff, R. S. *Nature Commun.* **2012**, *3*, 638−645.

(37) Fellinger, T.-P.; Hasché, F.; Strasser, P.; Antonietti, M. *J. Am. Chem. Soc.* **2012**, *134*, 4072−4075.

(38) Ai, K.; Liu, Y.; Ruan, C.; Lu, L.; Lu, G. *Adv. Mater.* **2013**, *25*, 998−1003.

(39) Leon y Leon, C. A.; Solar, J. M.; Calemma, V.; Radovic, L. R. *Carbon* **1992**, *30*, 797−811.

(40) Ikeda, T.; Boero, M.; Huang, S.-F.; Terakura, K.; Oshima, M.; Ozaki, J.-I. *J. Phys. Chem. C* **2008**, *112*, 14706−14709 See also ref 18..

(41) Zhang, L.; Niu, J.; Dai, L.; Xia, Z. *Langmuir* **2012**, *28*, 7542−7550.

(42) Kaukonen, M.; Kujala, R.; Kauppinen, E. *J. Phys. Chem. C* **2012**, *116*, 632−636.

(43) Wang, P.; Wang, Z.; Jia, L.; Xiao, Z. *Phys. Chem. Chem. Phys.* **2009**, *11*, 2730−2740.

(44) Luo, Z.; Lim, S.; Tian, Z.; Shang, J.; Lai, L.; MacDonald, B.; Fu, C.; Shen, Z.; Yu, T.; Lin, J. *J. Mater. Chem.* **2011**, *21*, 8038−8044.

(45) Wang, L.; Ambrosi, A.; Pumera, M. *Angew. Chem., Int. Ed.* **2013**, *52*, 13818−13821 and refs cited therein.

(46) Masa, J.; Zhao, A.; Xia, W.; Sunb, Z.; Mei, B.; Muhler, M.; Schuhmann, W. *Electrochem. Commun.* **2013**, *34*, 113−116.

(47) Sharifi, T.; Nitze, F.; Berzaghui, H. R.; Tai, C. W.; Mazurkiewicz, M.; Malopeszy, A.; Stobinski, L.; Wågberg, T. *Carbon* **2012**, *50*, 3535−3541.

(48) Maldonado, S.; Morin, S.; Stevenson, K. J. *Carbon* **2006**, *44*, 1429−1437.

(49) Glerup, M.; Castignolles, M.; Holzinger, M.; Hug, G.; Loiseau, A.; Bernier, P. *Chem. Commun.* **2003**, 2542−2543.

(50) Terrones, M.; Ajayan, P. M.; Banhart, F.; Blase, X.; Carroll, D. L.; Charlier, J. C.; Czerw, R.; Foley, B.; Grobert, N.; Kamalakaran, R.; Kohler-Redlich, P.; Rühle, M.; Seeger, T.; Terrones, H. *Appl. Phys. A: Mater. Sci. Process.* **2002**, *74*, 355−361.

(51) Chizari, K.; Vena, A.; Laurentius, L.; Sundararaj, U. *Carbon* **2014**, *68*, 369−379.

(52) van Dommele, S.; Romero-Izquirdo, A.; Brydson, R.; de Jong, K. P.; Bitter, J. H. *Carbon* **2008**, *46*, 138−148.

(53) Lai, L.; Potts, J. R.; Zhan, D.; Wang, L.; Poh, C. K.; Tang, C.; Gong, K.; Shen, Z.; Linc, J.; Ruoff, R. S. *Energy Environ. Sci.* **2012**, *5*, 7936−7942.

(54) Sharifi, T.; Hu, G.; Jia, X.; Wågberg, T. *ACS Nano* **2012**, *10*, 8904−8912.

(55) Matter, P. H.; Zhang, L.; Ozkan, U. S. *J. Catal.* **2006**, *239*, 83−96.

(56) For a selection of recent papers dealing with N-doped carbon nanomaterials where pyridinic-N atoms are assumed to be the most catalytically active sites in the ORR, see: Kundu, S.; Chikka Nagaiah, T.; Xia, W.; Wang, Y.; van Dommele, S.; Hendrik Bitter, J.; Santa, M.; Grundmeier, G.; Bron, M.; Schuhmann, W.; Muhler, M. *J. Phys. Chem. C* **2009**, *113*, 14302−14310 and refs 57−61.

(57) Rao, C. V.; Cabrera, C. R.; Ishikawa, Y. *J. Phys. Chem. Lett.* **2010**, *1*, 2622−2627.

(58) Subramanian, N. P.; Li, X.; Nallathambi, V.; Kumaraguru, S. P.; Colon-Mercado, H.; Wu, G.; Lee, J.-W.; Popov, B. N. *J. Power Sources* **2009**, *188*, 38−44.

(59) Park, K. Y.; Jang, J. H.; Hong, J. E.; Kwon, Y. U. *J. Phys. Chem. C* **2012**, *116*, 16848−16853.

(60) Li, H. B.; Kang, W. J.; Wang, L.; Yue, Q. L.; Xu, S. L.; Wang, H. S.; Liu, J. F. *Carbon* **2013**, *54*, 249−257.

(61) Jeyabharathi, C.; Venkateshkumar, P.; Rao, M. S.; Mathiyarasu, J.; Phani, K. L. N. *Electrochim. Acta* **2012**, *74*, 171−175.

(62) For a selection of recent papers dealing with N-doped carbon nanomaterials where graphitic N atoms are considered the most catalytically active sites in the ORR, see: Niwa, H.; Horiba, K.; Harada, Y.; Oshima, M.; Ikeda, T.; Terakura, K.; Ozaki, J.-I.; Miyata, S. *J. Power Sources* **2009**, *187*, 93−97 and refs 20, 21, 40, 53, 63, and 64.

(63) Zheng, B.; Wang, J.; Wang, F. B.; Xia, X. H. *Electrochem. Commun.* **2013**, *28*, 24−26.

(64) Chokai, M.; Taniguchi, M.; Moriya, S.; Matsubayashi, K.; Shinoda, T.; Nabae, Y.; Kuroki, S.; Hayakawa, T.; Kakimoto, M.; Ozaki, J.; Miyata, S. *J. Power Sources* **2010**, *195*, 5947−5951.

(65) For selected papers where both graphitic and pyridinic N atoms are suggested to be active in ORR, see: refs 53 and 54.

(66) For examples of N-CNMs active in the ORR where the catalyst efficiency does not seem to be affected by the overall N-content, see: Biddinger, E. J.; Ozkan, U. S. *J. Phys. Chem. C* **2010**, *114*, 15306−15314 and refs 53 and 67.

(67) Zhao, A.; Masa, J.; Muhler, M.; Schuhmann, W.; Xia, W. *Electrochim. Acta* **2013**, *98*, 139−145.

(68) For examples of N-CNMs active in the ORR where the catalyst efficiency is affected by the overall N-content, see: Deng, D.; Pan, X.; Yu, L.; Cui, Y.; Jiang, Y.; Qi, J.; Li, W.-X.; Fu, Q.; Ma, X.; Xue, Q.; Sun, G.; Bao, X. *Chem. Mater.* **2011**, *23*, 1188−1193 and ref 69.

(69) Zhang, Y.; Ge, J.; Wang, L.; Wang, D.; Ding, F.; Tao, X.; Chen, W. *Sci. Rep.* **2013**, *3*, 2771−2779.

(70) Sidik, R. A.; Anderson, A. B.; Subramanian, N. P.; Kumaraguru, S. P.; Popov, B. N. *J. Phys. Chem. B* **2006**, *110*, 1787−1793.

(71) Tuci, G.; Zafferoni, C.; D'Ambrosio, P.; Caporali, S.; Ceppatelli, M.; Rossin, A.; Tsoufis, T.; Innocenti, M.; Giambastiani, G. *ACS Catal.* **2013**, *3*, 2108−2111.

(72) Perrin, D. D.; Armarego, W. L. F.; Perrin, D. R. *Purification of Laboratory Chemicals*, 2nd ed.; Pergamon: New York, 1980; Vol. 1.

(73) Ferrari, A. C.; Robertson, J. *Phys. Rev. B* **2000**, *61*, 14095−14107.

(74) Ferrari, A. C.; Robertson, J. *Phys. Rev. B* **2001**, *64*, 075414.

(75) Lucchese, M. M.; Stavale, F.; Martins Ferreira, E. H.; Vilani, C.; Moutinho, M. V. O.; Capaz, R. B.; Achete, C. A.; Jorio, A. *Carbon* **2010**, *48*, 1592−1597.

(76) Treimer, S.; Tang, A.; Johnson, D. C. *Electroanalysis* **2002**, *14*, 165−171.

(77) For titration procedures, see: (a) Ballesteros, B.; de la Torre, G.; Ehli, C.; Aminur Rahman, G. M.; Agulló-Rueda, F.; Guldi, D. M.; Torres, T. *J. Am. Chem. Soc.* **2007**, *129*, 5061−5068 and ref 78.

(78) Moaseri, E.; Baniadam, M.; Maghrebi, M.; Karimi, M. *Chem. Phys. Lett.* **2013**, *555*, 164−167.

(79) Frisch, M. J. et al. *Gaussian09, Revision C.01*, Gaussian Inc., Wallingford, CT, 2010.

(80) Becke, A. D. *J. Chem. Phys.* **1993**, *98*, 5648−5652.

(81) Grimme, S.; Antony, J.; Ehrlich, S.; Krieg, H. *J. Chem. Phys.* **2010**, *132*, 154104.

(82) Tang, W.; Sanville, E.; Henkelman, G. *J. Phys.: Condens. Matter* **2009**, *21*, 084204.

(83) Bahr, J. L.; Tour, J. M. *Chem. Mater.* **2001**, *13*, 3823−3824.

(84) Dyke, C. A.; Tour, J. M. *J. Am. Chem. Soc.* **2003**, *125*, 1156−1157.

(85) Dyke, C. A.; Tour, J. M. *Nano Lett.* **2003**, *3*, 1215−1218.

(86) Hudson, J. L.; Casavant, M. J.; Tour, J. M. *J. Am. Chem. Soc.* **2004**, *126*, 11158−11159.

(87) Dyke, C. A.; Stewart, M. P.; Maya, F.; Tour, J. M. *Synlett* **2004**, *1*, 155−160.

(88) Price, B. K.; Hudson, J. L.; Tour, J. M. *J. Am. Chem. Soc.* **2005**, *127*, 14867−14870.

(89) Price, B. K.; Tour, J. M. *J. Am. Chem. Soc.* **2006**, *128*, 12899−12904.

(90) Doyle, C. D.; Tour, J. M. *Carbon* **2009**, *47*, 3215−3218.

(91) Lipińska, M. E.; Rebelo, S. L. H.; Pereira, M. F. R.; Gomes, J. A. N. F.; Freire, C.; Figueiredo, J. L. *Carbon* **2012**, *50*, 3280−3294.

(92) Chizari, K.; Janowska, I.; Houllé, M.; Florea, I.; Ersen, O.; Romero, T.; Bernhardt, P.; Ledoux, M. J.; Pham-Huu, C. *Appl. Catal. A: Gen.* **2010**, *380*, 72−80.

(93) Dalettoua, M. K.; Paloukisa, F.; Stefopoulosa, A. *ECS Trans.* **2009**, *25*, 1915−1924.

(94) de Villeneuve, C. H.; Pinson, J.; Bernard, M. C.; Allongue, P. *J. Phys. Chem. B* **1997**, *101*, 2415−2420.

(95) Bard, A. J.; Faulkner, L. R. *Electrochemical Methods: Fundamentals and Applications*, 2nd ed.; John Wiley & Sons, Inc.: New York, 2001; p 856.

(96) Bader, R. *Atoms in Molecules: A Quantum Theory*; Oxford University Press: Cary, NC, 1994.

(97) Calculations have been performed on the isolated heterocycles ($N_1−N_6$) as simplified models, focusing on N-charge and C_α-charge values; none of the largely unpredictable electronic contributions from the CNM have been taken into account.

(98) Shi, Z.; Zhang, J.; Liu, Z.; Wang, H.; Wilkinson, D. *Electrochim. Acta* **2006**, *51*, 1905−1916.